INTERNATIONAL ATOMIC ENERGY AGENCY
UNITED NATIONS EDUCATIONAL, SCIENTIFIC AND CULTURAL ORGANIZATION
INTERNATIONAL CENTRE FOR THEORETICAL PHYSICS
I.C.T.P., P.O. BOX 586, 34100 TRIESTE, ITALY, CABLE: CENTRATOM TRIESTE

H4.SMR/453-5

TRAINING COLLEGE ON PHYSICS AND CHARACTERIZATION OF LASERS AND OPTICAL FIBRES

(5 February - 2 March 1990)

Radiance-ratio Algorithm Wavelengths for Remote Oceanic Chlorophyll Determination

F. Hoge

NASA Goddard Space Flight Center
Wallops Flight Facility
Wallops Island, Virginia
U.S.A.

Radiance-ratio algorithm wavelengths for remote oceanic chlorophyll determination

Frank E. Hoge, C. Wayne Wright, and Robert N. Swift

a reprint from Applied Optics
volume 26 number 11, June 1, 1987

Radiance-ratio algorithm wavelengths for remote oceanic chlorophyll determination

Frank E. Hoge, C. Wayne Wright, and Robert N. Swift

Two-band radiance-ratio in-water algorithms in the visible spectrum have been evaluated for remote oceanic chlorophyll determination. Airborne active–passive (laser–solar) data from coastal, shelf-slope, and blue-water regions were used to generate 2-D chlorophyll-fluorescence and radiance-ratio statistical correlation matrices containing all possible two-band ratio combinations from the thirty-two available contiguous 11.25-nm passive bands. The principal finding was that closely spaced radiance-ratio bands yield chlorophyll estimates which are highly correlated with laser-induced chlorophyll fluorescence within several distinct regions of the ocean color spectrum. Band combinations in the yellow (~565/575-nm), orange-red (~675/685-nm), and red (~695/705-nm) spectral regions showed considerable promise for satisfactory chlorophyll pigment estimation in near-coastal Case II waters. Based on very limited data, pigment recovery in Case I waters was best accomplished using blue-green radiance ratios in the ~490/500-nm region.

I. Introduction

This paper describes recent efforts to find improved in-water two-band radiance-ratio algorithms for chlorophyll pigment concentration measurement. While two-band differences, slopes, and ratios have all been considered for chlorophyll measurement, the ratio method is presently the most widely used. The studies herein were primarily directed toward coastal regions having a high probability of containing Case II waters.[1] Active–passive (laser–solar) correlation spectroscopy methods were applied over the visible ocean color spectrum to systematically evaluate hundreds of algorithms. Summary results of this analytical investigation are presented following a brief review of the evolution of the ocean color radiance-ratio algorithm, the airborne instrumentation, and the active–passive spectroscopy methodology.

The radiance-ratio algorithm is today the mainstay of satellite ocean color remote sensing. Characterized by empirical simplicity, it is used to estimate chlorophyll, seston, and water attenuation.[1] By straightforward statistical analysis of shipboard data, two linear regression coefficients are determined for a desired property, say chlorophyll. Then, depending on the type of water being observed, a pair of spectral bands and appropriate coefficients are selected to calculate the chlorophyll concentration from the atmospherically corrected satellite measured radiances. The success of the radiance-ratio method for estimating oceanic chlorophyll concentration has been remarkable when one considers the complexity of the vast biogeochemical processes that drive the observed color spectrum.

The radiance-ratio algorithm is important for several other reasons. Because of the complexity of the ocean color processes as viewed through the atmosphere, no one has ever recommended use of a single-band algorithm. Thus two bands are probably the minimum number necessary to recover a water column constituent under varied conditions. From an engineering and/or economic standpoint, the two-band sensor requires minimum data transmission, storage, reduction, and algorithm application requirements to obtain the water constituents and/or water optical properties. This can lead to significant economic benefits for spaceborne sensor design and instrumentation. Of the two-band possibilities, the radiance ratio (as opposed to radiance difference or radiance slope) does not demand exceptional measurement precision. The two-band radiance ratio has a normalizing property caused by the division of the radiance from a longer wavelength channel.

The radiance-ratio algorithm evolved over a time period exceeding one decade. In 1968 Ramsey[2] discussed several remote sensing chlorophyll measurement schemes, one of which was the use of the ra-

Robert Swift is with EG&G Washington Analytical Services, Inc., Pocomoke, Maryland 21851; the other authors are with NASA Goddard Space Flight Center, Wallops Flight Facility, Wallops Island, Virginia 23337.

Received 15 December 1986.

diances in the 470- and 540-nm bands. He did not specify whether the bands were to be used in a difference, slope, or ratio calculation. Jerlov[3] reported the construction in 1969 of a two-band color meter which used the ratio of the 450- and 520-nm bands as a color index. The meter was not deployed until 1971. In their landmark paper, Clarke *et al.*[4] indicated that changes in the slope of their airborne spectral radiances correlated quite closely with differences in chlorophyll concentration. Clarke and Ewing[5] reported use of a 540/460-nm color ratio for experiments beginning in 1969. This color ratio was later adopted by Curran[6] and Arvesen *et al.*[7] Later Arvesen *et. al.*[8] successfully used the 443- and 525-nm bands in a differential radiometer mode. Ramsey and White[9] and Hovis and Leung[10] likewise chose a two-band radiance ratio to infer chlorophyll. Clarke and Ewing[5] credit the color ratio scheme to Strickland[11] who used a more sophisticated form to normalize the blue and green energy to that in the red.

Use of the radiance ratio to infer chlorophyll was solidified by the findings of Morel and Prieur.[12] They showed that the ratio of the irradiance reflectances at 440 and 560 nm and the chlorophyll plus phaeophytin *a* (hereafter called chlorophyll) concentration yielded a crude linear relationship when plotted in the log–log domain. This latter finding eventually led to the present-day power-law algorithm, which will be subsequently discussed in more detail. Their choice of the wavelengths for the chlorophyll algorithm was not arbitrary but was predicated on known physical processes such as absorption. The specific wavelengths selected by Morel and Prieur[12] were based on the respective absorption maximum at 440 nm and absorption minimum at 560 nm.

This paper describes results from a systematic investigation of radiance-ratio combinations for estimating chlorophyll concentration regardless of the causative physical processes. However, the physical processes are usually identifiable. The efforts herein are in partial response to a standing recommendation by the Working Group on Ocean Color who suggested that a continuing program be directed toward establishing a data base to enlarge the applicability of the general algorithm [to be used by NASA to carry out basic Coastal Zone Color Scanner (CZCS) processing] and to aid in development of more accurate algorithms.[13] The wavelength investigations here are directed toward improved in-water or biooptical algorithms without immediate concern for their suitability for correction of other effects such as scattered radiance from the atmosphere. Furthermore, since satisfactory algorithms are presently available for Case I waters, the efforts described herein were primarily focused on Case II waters.

II. Radiance-Ratio Algorithm for Oceanic Chlorophyll

Morel and Prieur[12] presented a log–log graph of the irradiance reflectance ratio $R(440)/R(560)$ vs the chlorophyll *a* (plus phaeopigment *a*) concentration C in mg/m^3. A generally linear relationship was obtained. This suggests a power law of the form

$$C = Ar_{ij}^{B}, \tag{1}$$

where r_{ij} = reflectance at wavelength λ_i/reflectance at a longer wavelength λ_j, and A and B are constants to be determined by linear regression in the log–log domain.

Satellite remote sensors do not, however, measure reflectance but instead measure upwelling radiances. Fortunately, the two measurements are related by a geometrical factor.[14] This factor is slightly dependent on wavelength, and its variability is generally felt to be small.[1] Accordingly, remotely measured radiances will be directly used rather than reflectance. Furthermore, since in-water algorithms are of interest here, water-leaving radiances will be utilized in the calculations, since the observed total radiance recorded onboard the aircraft contains unwanted atmospheric path radiances and reflected sky-radiance contributions.

The form of Eq. (1) has been routinely used for estimating chlorophyll concentration levels from CZCS imagery using band ratios at 443/550 and 520/550 nm. We assume in this analysis that the generally linear relationship between r_{ij} and chlorophyll pigment C is maintained for all available radiance ratios of the ocean color spectrum. The extent to which the r_{ij}-chlorophyll fluorescence relationship deviates from linear is not addressed.

A. Classical Shipboard Algorithm Data Acquisition

Conventionally, the correlation coefficient and the recovery of the regression coefficients A and B require tens if not hundreds of pairs of chlorophyll pigment and radiance-ratio measurements obtained by shipboard instruments in numerous global locations. An example of the desired spatial diversity of the measurements is given in a paper by Gordon *et al.*[15] Generally, chlorophyll concentration is obtained by direct measurement of a water sample along with concurrent radiance measurements. These point measurements of chlorophyll are sometimes supplemented by underway fluorometry determinations of the pigment concentration. The amount and diversity of such truth data are essentially limited by the speed of the surface vessel.

B. Airborne Data Acquisition

Recently, airborne laser systems have demonstrated that chlorophyll *a* and phycoerythrin fluorescence along with laser-induced water Raman backscatter can be reliably measured over wide areas of the ocean both rapidly and at a high sample density.[16–19] Hardware improvements to the NASA airborne oceanographic lidar (AOL) implemented over the past two years have enabled the instrument to acquire simultaneous active and passive ocean color measurements.[20,21] The voluminous laser-induced and solar-induced spectra synoptically available from essentially the same footprint permit studies of the variability of ocean color spectral

Table I. AOL–POCS Parameters

Transmitter:	
Wavelength	532 nm
Pulse width	15 ns
Pulse rate	6.25 pps
Peak output power (max)	≤3 MW
Beam divergence	0.2–2 mrad[a] (adjustable)
Receiver	
Bandwidth	350–800 nm[b] (32 channels)
Spectral resolution (min)	11.25 nm
Field of view (FOV)	1–20 mrad,[c] variable, vertical and horizontal

[a] Approximate 2-mrad beam divergence was utilized for the experiments discussed herein.

[b] The thirty-two contiguous fluorosensor channels provide a 360-nm bandwidth which can be placed between 350 and 800 nm.

[c] A 2 × 5- or 2 × 7-mrad FOV was utilized for the experiments discussed herein.

radiance and subsequent development of algorithms. A typical airborne flight mission produces ~50,000 pairs of active–passive observations.

C. Validity of Airborne Active–Passive Methods

The airborne laser-induced chlorophyll fluorescence from the water column has been shown to yield a high correlation with the pigment concentration as derived by shipboard extractions and underway fluorescence.[16,22,23] These findings are in spite of known chlorophyll fluorescence variability caused by ambient light and nutrient changes.[24] The effects of solar photoinhibition on airborne laser-induced chlorophyll fluorescence have been reported.[25] However, our observations indicate that this effect is not evident in data sets acquired in relatively cloudless conditions over a relatively short 2–3 h period. Thus, with the singular assumption that the airborne laser-induced chlorophyll *a* fluorescence is a reliable indicator of the pigment concentration, it will be used as the sole source of data for identification and evaluation of radiance-ratio chlorophyll algorithm spectral regions.

III. Instrumentation and Airborne Field Experiments

The AOL with its integral passive ocean color subsystem (POCS) was used to obtain the field data presented here. The AOL has been discussed in detail in papers dealing with various marine applications including other chlorophyll mapping field experiments[16–19] as well as oil spill,[26,27] tracer dye,[28] oceanic turbidity cell structure,[29] water depth,[30] and laser backscatter[31,32] measurement investigations. The AOL is also capable of performing terrestrial investigations[33,34] including leaf fluorescence.[35] The POCS instrumentation subsystem has been recently described in detail.[20] Its application to the airborne measurement of oceanic pigments has also been given.[21] Together, the AOL–POCS functions as an effective active–passive ocean color measurement system.[20,21] The system yields active–passive data which will be utilized in an effective technique known as active–passive correlation spectroscopy.[36] Principal features

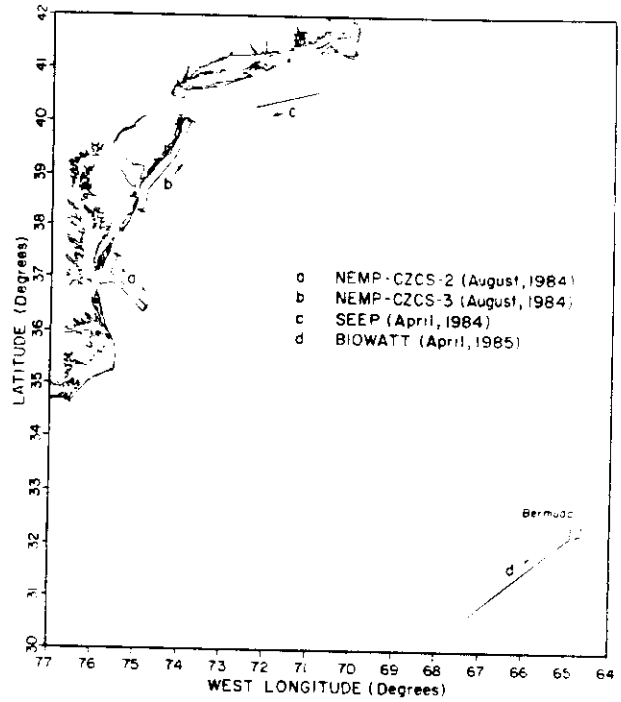

Fig. 1. Map showing the locations of flight lines selected for analysis in the two-band radiance-ratio study. The individual flight lines are designated with small letters, while the flight direction is indicated by arrows. The name of the field experiment flight mission associated with each of the flight lines is shown within the figure.

of the AOL–POCS are given in Table I.

The airborne ocean color data were acquired from a NASA P-3 aircraft flying ~150 m above the ocean surface. The AOL final mirror was adjusted so that the ocean was viewed at an off-nadir angle of 15° and azimuthally away from the sun.

The data herein were obtained during the execution of several airborne field experiments in the northwestern Atlantic Ocean. The missions were part of three separate investigations called (1) NEMP-CZCS, (2) SEEP, and (3) BIOWATT.

The NOAA-CZCS airborne field experiments were conducted during Aug. 1984 in coordination with the (1) National Oceanic and Atmospheric Administration (NOAA) North East Monitoring Program (NEMP) and (2) NOAA–CZCS calibration. Two passes from the series of four flight missions have been selected for consideration in this investigation. The locations of these two passes are designated in Fig. 1 as *a* and *b*. Both flight lines were conducted over Case II waters.

Surface truthing measurements of chlorophyll were obtained during these investigations from the R/V Cape Henlopen by the NOAA/NEMP investigators. Unfortunately, due to several logistical problems over which we had no control, many of the ship and aircraft observations were not coincident in either time or space. Thus a large portion of the truthing data obtained during the NOAA–CZCS airborne field experiments is not concurrent enough to utilize for verifying individual measurements of laser-induced chlorophyll

fluorescence. However, in most cases, the separation in time and space is small enough to permit the truthing measurements to be utilized to some extent for verifying the range of pigment concentration within certain study areas.

The shelf edge exchange processes (SEEP) flights were conducted in the New York Bight as part of a Department of Energy (DOE) program designed to assess the assimilative capacity of the continental shelf to absorb energy by-products introduced into the nearshore ocean environment from coastal communities and marine activities such as offshore oil operations. One pass acquired from the inner portion of the SEEP study site during a mission flown on 2 Apr. 1984 was chosen for analysis in this study. Its location is identified in Fig. 1 by the letter c. This water was not typed but is felt to be Case II waters that may have been advected into a typically Case I region by a sustained strong westerly wind event the day prior to the flight. No reasonably concurrent surface chlorophyll measurements are available for the aircraft data acquired on flight line *c*. The research vessel was operating in another portion of the SEEP study site at the time the aircraft observations were acquired along flight line *c*.

The BIOWATT airborne missions were flown in support of a Navy program to study bioluminescence and the optical variability of the ocean, as principally driven by plankton population.[37] These experiments were conducted in Case I waters as shown. The flight line (identified as *d* in Fig. 1) was located SW of Bermuda and flown on 16 Apr. 1985. No supporting surface truth observations were acquired in the area of flight line *d*.

The present CZCS sensor and two-band ratio algorithms r_{ij} = 443/550 nm and 520/550 nm recover chlorophyll quite well in Case I waters.[1,15] Accordingly, our efforts are principally focused on Case II waters and the need for more effective algorithms there. The Case I example is offered herein primarily for the purpose of comparison.

The data from the above field missions were evaluated for several important criteria prior to beginning the analysis with the active–passive correlation spectroscopy technique described in the next section. Specifically, these criteria were:

(1) Only those flight lines that provided a reasonably wide range of chlorophyll concentration were selected. The linear regression process requires a sufficient variation in the variables to yield an accurate solution.

(2) Only passes which contained distinct sections where the concentration of chlorophyll was found to be noncoherent with the concentration of phycoerythrin were considered for this analysis. This precaution was adopted to assure that the chlorophyll algorithms are not responding to phycoerythrin which often covaries with chlorophyll. Phycoerythrin is the other phytoplankton photopigment which is currently measurable with the AOL using a laser excitation wavelength of 532 nm.

(3) Passes were selected which exhibited some small-scale variability or patchiness. The relatively small 1–10-km patches of elevated chlorophyll concentration provide excellent visual contrast between profiles of laser-induced chlorophyll fluorescence and estimates of chlorophyll concentration developed following application of the active–passive correlation spectroscopy technique.

(4) Only data which were free of sun glint or glitter were retained for further analysis. Those data found to meet the first three criteria were then edited to remove from consideration those spectra which were contaminated with sun glint. Only passes which required the removal of 10% or fewer observations were ultimately used for analysis.

During each flight mission a considerable amount of active and passive data is actually acquired. However, only a very small subset is found to meet the above criteria for use in the analyses.

Prior to further analysis the data were averaged to reduce the volume of samples and to partially smooth high-frequency variability. The laser-induced fluorescence observations which were acquired at 6.25 samples/s were subjected to a ten-point simple average. The passive ocean color spectra which were acquired at a rate of 12.5 samples/s were averaged over the same 1.6-s time interval (after removal of observations containing sun glint). At the nominal 100-m/s velocity of the aircraft, this process effectively averages the samples over a space of 160 m. A more comprehensive treatment of the data handling can be found in Ref. 21.

IV. Active–Passive Correlation Spectroscopy Methods

Briefly, active–passive correlation spectroscopy (APCS) is a highly sensitive technique which allows subtle constituent-driven variations in the airborne ocean color spectrum to be easily detected.[36] During postflight analysis, all possible radiance ratio combinations from the thirty-two available passive color bands of the instrument were used to compute independent chlorophyll concentration estimates. (The actual methodology is presented in more detail in the following section.) Each of the resulting 496 radiance ratios were then linearly regressed against the AOL laser-induced and water-Raman-normalized chlorophyll fluorescence for each sampling point along the flight line. High regression coefficients ($\rho > 0.80$) revealed those regions of the spectrum where the ocean color spectral variability was strongly correlated with the chlorophyll fluorescence. The APCS technique was recently used to find three regions of the ocean color spectrum, 460–510, 645–660, and 680–695 nm,[36] where the spectral curvature algorithm[38–40] can be fruitfully applied for chlorophyll pigment estimation.

A. Reflected Sky-Radiance Corrections

The correlation technique is effective since it examines the passive ocean color spectrum for responses or variations which are related only to the presence of the chlorophyll pigment (as indicated by laser-induced

fluorescence). From this standpoint, other variations which are not associated with chlorophyll pigment are basically disregarded. The reflected sky spectral radiance is very nearly constant during the time period of a single airborne flight line (~15 min). The sky radiance can in turn be modulated by surface gravity and capillary waves. However, these sky-radiance variations are essentially uncorrelated with the chlorophyll pigment content. Other variations in the ocean color spectrum are similarly disregarded by the correlation process. However, to maintain as much completeness as possible a straightforward sky-radiance correction was made to the upwelled spectral data.

The total sensor radiance detected by the airborne radiometer $L_T(\lambda)$ is composed of (a) the water-leaving contribution which contains the desired ocean color contributions $L_W(\lambda)$; (b) the sky radiance $L_S(\lambda)$ specularly reflected at the ocean surface toward the airborne sensor; and (c) the sensor-to-pixel path radiance scattered toward the sensor by the atmosphere and its constituents including aerosols. The undesirable reflected sky radiance $L_s(\lambda)$ must be subtracted from the total radiance detected by the passive spectroradiometer. The path radiance contribution is small[41] for our low-flight altitude, especially in the rather clear atmospheric conditions existing during our airborne experiments. Accordingly, it will be neglected. Also, the atmospheric attenuation of the water-leaving and reflected sky radiances is assumed to be neglectable for our 150-m flight altitude. The water-leaving radiance $L_W(\lambda)$ is thus

$$L_W(\lambda) = L_T(\lambda) - r_d L_S(\lambda), \tag{2}$$

where r_d is the effective Fresnel reflectance for the observing angle and wind speed during the field experiment. After consideration of the wind speed and direction obtained via the aircraft inertial navigation system, a value of 0.021 for the reflectance r_d was used.[42] Likewise, since the sky radiance $L_S(\lambda)$ was not measured during the experiment, representative values were obtained from the data of Austin.[42] The total spectral radiance $L_T(\lambda)$ at the sensor was then corrected for reflected sky radiance according to Eq. (2). The water-leaving radiances $L_W(\lambda)$ were used exclusively to compute the passive r_{ij} or radiance-ratio values, which were in turn regressed against the laser-induced and water-Raman-normalized chlorophyll fluorescence measurements. The sky-radiance correction had only a modest effect on the computed radiance ratios and their correlation with the laser-induced fluorescence. However, the effect on the computed regression coefficients A, B in Eq. (1) was found to be considerable. Accordingly, experiments aimed primarily at developing the actual in-water algorithm would have to be designed to allow far more rigorous reflected radiance corrections. Our efforts were confined to algorithm wavelength determinations.

V. Radiance-Ratio Algorithm Wavelength Determination Using Active–Passive Correlation Spectroscopy

The log form of Eq. (1) is

$$\log C = \log A + B \log r_{ij}. \tag{3}$$

The chlorophyll C is obtained from the AOL laser-induced and water-Raman-normalized chlorophyll fluorescence, while the radiances are obtained from the POCS. Specifically, the laser-induced fluorescence spectrum[16,19] is denoted $F(\lambda_i)$, where λ_i is the midpoint of each of the thirty-two calibrated bands of the AOL. The water-Raman-normalized spectrum $F'(\lambda_i)$ is formed by dividing $F(\lambda_i)$ by the signal at the water-Raman wavelength $F(\lambda_R)$. Thus $F'(\lambda_i) = F(\lambda_i)/F(\lambda_R)$. If at the chlorophyll emission wavelength $\lambda_i = \lambda_c = 685$ nm the signal is $F(\lambda_c) = F_c$ and at the Raman wavelength λ_R the signal is $F(\lambda_R) = R$, then simply $F' = F_c/R$. Since laser-induced fluorescence has been found to be linearly correlated to the chlorophyll concentration,[16,40,43] the chlorophyll pigment concentration is adequately modeled by the linear relationship[44]

$$C = a + bF', \tag{4}$$

where a is the background fluorescence and/or instrument bias and b is the slope of an F' vs C regression. The 532-nm laser-induced fluorescence spectrum contains little or no background. A small amount of digitizer bias is removed during calibration.[16] Thus $C = bF'$. Then from Eqs. (3) and (4)

$$\log F' = \log\frac{A}{b} + B \log r_{ij}. \tag{5}$$

The linear regression of the laser-induced and water-Raman-normalized chlorophyll fluorescence F' and the radiance ratio r_{ij} yields a correlation coefficient ρ_{ij} and the constants $\log(A/b)$ and B.

For N radiometer spectral bands the radiance-ratio/chlorophyll-fluorescence correlation matrix is

$$\rho i,j = \begin{pmatrix} \rho_{1,1} & \rho_{1,2} & \rho_{1,3} \cdots \rho_{1,N} \\ & \rho_{2,2} & \rho_{2,3} \cdots \rho_{2,N} \\ & & \rho_{3,3} \cdots \rho_{3,N} \\ & & \vdots \\ \text{(symmetric)} & & \rho_{N,N} \end{pmatrix}. \tag{6}$$

When $i = j$, a spectral band is being ratioed with itself to yield $\rho_{ij} = 1$. For this condition $\log F'$ would be regressed against $\log r_{ij} = 0$. Accordingly, we have set $\rho_{ij} = 0$ for $i = j$ and utilize only the meaningful off-diagonal elements, $i \neq j$. Band i is the short wavelength, and band j is the long wavelength or normalizing band. Note that the wavelength spacing ($\Delta\lambda_{ij} = \lambda_j - \lambda_i$) increases as one departs further from the diagonal. Likewise, closely spaced bands occupy regions nearer the diagonal. Of course, for any particular diagonal $\lambda_j - \lambda_i$ = constant.

Essentially, if $L_m(\lambda_k)$ are the water-leaving radiances in k spectral bands corresponding to m different chlorophyll concentrations C_m (or laser-induced fluorescence levels F_m), one is essentially mapping the L, C_m, λ_k space into ρ, λ_i, λ_j space. The mapping or transformation is accomplished via the empirical statistical correlation required by the power law algorithm in Eq. (1) [or its fluorescence analog in Eq. (5)]. Here $i < j < k$.

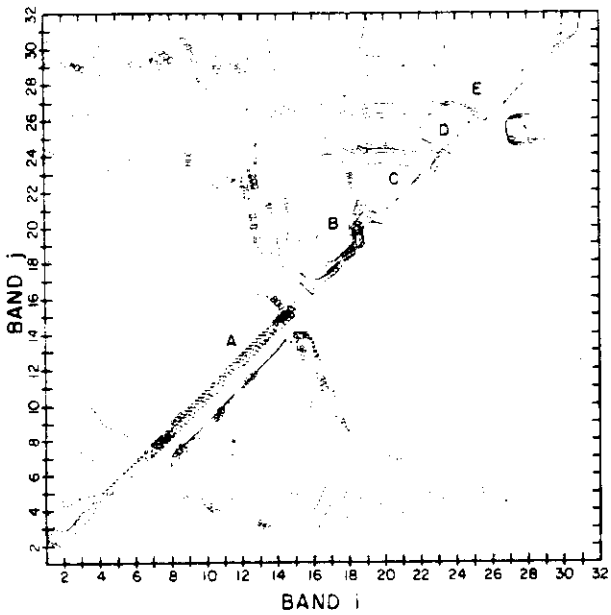

Fig. 2. Contour plot of the correlation coefficients obtained on flight line *a* (see Fig. 1) from the linear regression of the two-band radiance ratios against the laser-induced chlorophyll fluorescence. The section of the plot to the left of the diagonal is contoured in units of 0.1. The symmetric equivalent section to the right of the diagonal has been plotted in units of 0.01 to provide additional definition in areas where the absolute values of the correlation coefficients were found to be >0.9. The regions of highest correlation are labeled with capital letters to facilitate discussion within the text. The midpoint wavelength of channels 1 and 32 are 413.75 and 762.5 nm, respectively.

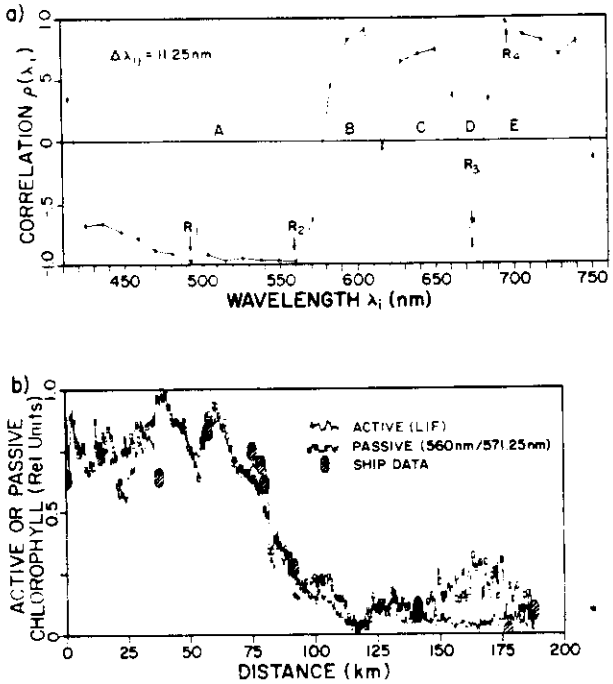

Fig. 3. (a) Spectral correlation function $\rho(\lambda_i)$ formed from the first off-diagonal elements ($\Delta\lambda_{ij}$ = 11.25 nm) of the matrix shown in Fig. 2. The regions of highest correlation (*A*, *B*, *C*, *D*, *E*) correspond to similarly labeled near-diagonal areas of Fig. 2. The two-band ratios chosen for the along-track profile plots in Figs. 4, 5, 6, and 7 are labeled R_1, R_2, R_3, and R_4. (b) Along-track profile of the laser-induced chlorophyll fluorescence and the 560/571.25-nm radiance ratio. Contemporaneous chlorophyll concentration measurements obtained from a cooperating research vessel are shown plotted as enlarged and shaded symbols within the figure.

VI. Description of Results

Results obtained from the analysis of data acquired from flight line *a* (Fig. 1) during the NOAA–CZCS airborne field experiments during Aug. 1984 will initially be discussed. The northernmost segment of flight line *a* is located within 3 km of the coast and thus is difficult to discern on the scale used in Fig. 1. The pass was flown from nearshore to offshore as can be seen by the labeling on the figure.

During the flight experiments the AOL system was configured to operate in the active–passive mode and record $N = 32$ contiguous bands, each having a width of ~11.25 nm. The 32-band data are discussed first. Subsequently, these bands were linearly and evenly interpolated to yield effectively $2N - 1$ or 63 bands whose separation was 5.625 nm. These spectrally interpolated data are then discussed.

Figure 2 shows the radiance-ratio/chlorophyll-fluorescence correlation matrix for the 415–760-nm spectral region. The correlation coefficients ρ have been contour plotted for ease of interpretation. The areas of highest correlation have been contoured in the symmetric or transdiagonal portion of the matrix to aid further in the analysis. As expected, broad areas of high correlation were found in the blue and blue-green spectral regions and are labeled *A* in Fig. 2. A second region of high correlation can be seen in the red spectral region and is labeled *E*. Surprisingly, and perhaps more important, these sections of high correlation extend into the area nearest the diagonal where adjacent contiguous channels were used in the calculation. This latter finding suggests that (1) important correlative information is contained in adjacent and nearly adjacent bands, and (2) it is, therefore, not necessary to choose widely separated bands for radiance-ratio algorithms. Advantageously, closely spaced color bands can then share an atmospheric correction procedure whose working values are more likely to be consistent due to the smaller wavelength separation interval.

Note that other areas of relatively high correlation with chlorophyll fluorescence can be seen in Fig. 2 at spectral regions labeled *B*, *C*, and *D* corresponding to ~605, 650, and 675 nm, respectively. These additional regions of high correlation are smaller and confined to the portion of the plot near the diagonal where the $\Delta\lambda_{ij}$ is small. As shall be subsequently discussed, the areas of high correlation (*A*,*E*) are related to chlorophyll absorption and chlorophyll fluorescence emission. To aid further in the interpretation of the radiance-ratio/chlorophyll-fluorescence correlation matrix, a plot of the off-diagonal elements for $\Delta\lambda_{ij}$ = 11.25 nm is shown in Fig. 3(a). As discussed previously, the AOL bands are contiguous and 11.25 nm wide. In Fig. 3(a) the correlation ρ is plotted as a function of the band i wavelength λ_i. The normalizing band at λ_j is 11.25 nm

redder or $\Delta\lambda_i$ = 11.25 nm. In correspondence to the area labeled *A* in the contour plot of Fig. 2, high correlations with the chlorophyll fluorescence are found for a broad region, 430–560 in the blue-green and yellow. Likewise, corresponding to regions *B*, *C*, *D*, and *E* in Fig. 2, high correlations are found at ~605, 650, 675, and 690 nm, respectively. The latter two regions of high radiance-ratio correlation at *D* and *E* are generally consistent with the results obtained when active–passive correlation spectroscopy methods were applied via the spectral curvature algorithm.[36] The correlation peaks found in the 605- and 650-nm regions [see *B* and *C* in Fig. 3(a)] have not been consistently and repeatedly found in the analysis of other data sets. Thus their occasional appearance [as in the correlation spectrum of Fig. 3(a)] is not as significant as are the correlation peaks at *A*, *D*, and *E*.

Figure 3(b) shows the 560/571.25-nm radiance-ratio algorithm plotted in profile form as a function of along-track distance (nearshore to offshore, flight line *a*) along with the laser-induced chlorophyll fluorescence profile. In this plot (as well as in subsequent cross sections) the log of the Raman normalized laser-induced chlorophyll fluorescence (solid line) has been autoscaled to run between relative units 0 and 1 as a convenient method for treating the data. The log of the chlorophyll estimate generated from the radiance-ratio algorithm (small connected symbols) has been plotted as a visual best-fit profile for ease of comparison. Due to the data density, only one symbol is plotted for every fourth value determined from the 160-m simple averaging performed during sample preprocessing. The correlation coefficient for the 560/571.25-nm band combination is shown as negatively correlated in Fig. 3(a). Accordingly, the radiance-ratio values were inverted in the Fig. 3(b) plot to allow improved comparison with the chlorophyll fluorescence profile. Also provided in Fig. 3(b) are the individual chlorophyll values determined from surface samples obtained by the NOAA/NEMP investigators onboard the R/V Cape Henlopen. The log values of these chlorophyll concentration measurements have been visually fitted to the autoscaled chlorophyll fluorescence profile and are shown plotted as larger unconnected symbols. The location of the NOAA/NEMP cruise track was nearly parallel to the aircraft flight line but was offset by 3–8 km. Also the ship and aircraft observations are separated in time by a period varying from <1 to more than 12 h. Thus the ship chlorophyll values should only be used to gauge the range of chlorophyll concentration rather than for determining the accuracy of individual laser observations. The actual chlorophyll concentration levels reported by the NOAA/NEMP investigators ranged between a low value of 0.08 μg/liter near 175 km to a high value of 7.6 μg/liter near 60 km.

The observed agreement with the chlorophyll fluorescence in Fig. 3(b) is generally typical of the closely spaced algorithms (nearest the diagonal) in segment A of Fig. 3(a). However, it should be pointed out that different algorithms with the same correlation coefficient relative to laser-induced chlorophyll fluorescence can yield good agreement in different geographical locations along a flight line. Accordingly, along-track or profile plots should be used to validate particular algorithms.

During previous active–passive correlation spectroscopy investigations, it was found that the use of intermediate bands, generated through interpolation of adjacent passive spectral bands, often improved results of the correlation technique.[36] Linear interpolation was again tried in this study and was found to generally produce slightly improved results. Accordingly, the remaining analysis in this investigation was performed with the original thirty-two bands and thirty-one intermediate bands created midway between the original bands through linear interpolation. Some caution should be used when interpreting the results, since up to four channels are involved as different possible combinations of the sixty-three channels are examined. In the case of calculations involving adjacent channels where an interpolated channel is ratioed with one of the original channels, the interpolation procedure merely provides more or less weight to one or the other of the original 11.25-nm width channels being used in the ratio. More complicated methods of weighting by polynomial fitting etc. can probably lead to some further improvement, but such techniques are beyond the scope of this paper.

Figure 4 shows along-track or cross-sectional profiles of representative closely spaced radiance-ratio algorithms (labeled *R*1, *R*2, *R*3, and *R*4) from each of the high spectral correlation sections *A*, *D*, and *E* shown in Fig. 3(a). Using the same format discussed in connection with Fig. 3(b), the logarithm of the 492.5/498.125-nm radiance ratio is shown plotted in Fig. 4(a) along with the logarithm of the laser-induced water-Raman-normalized chlorophyll fluorescence. This 493/498-nm ratio was chosen in particular from the broad segment *A* of Fig. 3(a) since it will be subsequently discussed in connection with some of the other flight lines. For simplicity, references to the wavelengths plotted in this and all subsequent profiles are rounded to the nearest nanometer since the fractional portion of a nanometer is not highly significant for a sensor whose bands are greater than 10 nm wide. Profiles of the other highly correlated radiance-ratio algorithms are shown in Figs. 4(b)–(d). These band combinations include 566/571, 673/678, and 695/701 nm. A profile of the Raman corrected chlorophyll fluorescence is included in each of the above figures to facilitate easier intercomparison of the results.

The logarithm of the Raman normalized phycoerythrin fluorescence is also plotted in Fig. 4(e) along with the log of the similarly corrected chlorophyll fluorescence profile. The relative strength of the two fluorescence profiles are correct as shown in Fig. 4(e). A reasonably large range in the concentration of the chlorophyll and phycoerythrin photopigments can be seen in the figure. Also apparent are areas of noncoherence between the two photopigments along the inner portion of the flight line between 0 and 80 km.

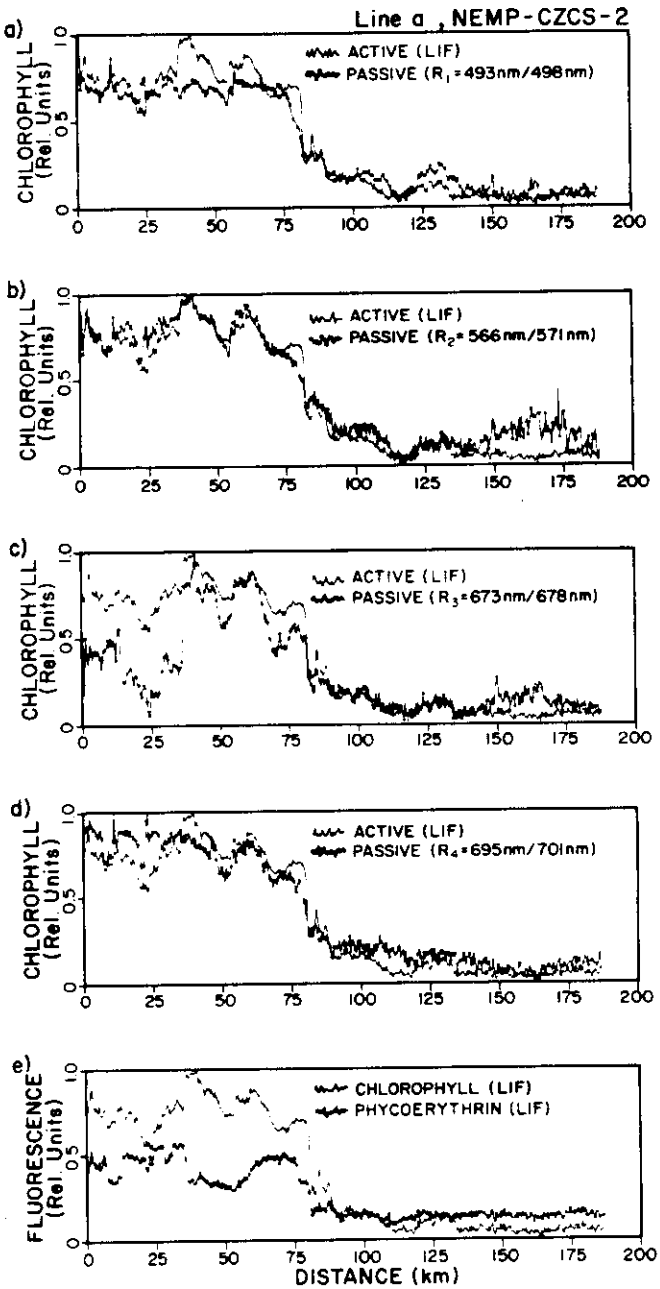

Fig. 4. (a)–(d) Along-track comparison of radiance ratios R_1, R_2, R_3, and R_4 with laser-induced chlorophyll fluorescence for flight line *a*. (e) Comparison of laser-induced phycoerythrin and chlorophyll fluorescence.

Table II provides the correlation coefficient for each of the radiance-ratio profiles given in Figs. 4(a)–(d). Also shown in Table II are the correlation coefficients for the 443/550 and 520/550 radiance-ratio band combinations that have been extensively used to extract chlorophyll concentration values from CZCS imagery. Because of the AOL spectrometer adjustment at the time of these experiments, it was not possible to select the exact wavelength corresponding to the 443-, 520-, and 550-nm bands. As a matter of convenience, 442 nm was substituted for 443, 521 nm for 520 nm and 549 nm for 550 nm, respectively. Plots of the radiance-

Table II. Correlation Coefficients for Selected Radiance Ratios

Flight line	Closely spaced band ratios R_1 493/498	R_2 566/571	R_3 673/678	R_4 695/701	CZCS band ratios 443/550	520/550[a]
a	−0.97	−0.97	−0.86	+0.96	−0.94	−0.98
b	−0.46	−0.76	−0.84	+0.47	−0.56	−0.75
c	−0.70	−0.94	−0.94	+0.84	−0.79	−0.88
d	−0.96	−0.51	−0.82	[b]	−0.95	−0.45

[a] The 520/550 band combination is applicable to mixtures of Case I and Case II waters (see ref. 15).

[b] These wavelengths not available with AOL spectrometer during the BIOWATT investigations.

ratio profiles from the CZCS band combinations are not given in this paper. As expected from Fig. 3(a) and Table II, the 566/571-nm radiance ratio [Fig. 4(b)] provided the best agreement over most of the flight line. However, notice that this band combination is less effective near the offshore end of the flight line. By contrast, the 493/498-nm algorithm in Fig. 4(a), which has nearly as good a correlation coefficient over the entire flight line, shows better agreement offshore than in the nearshore high chlorophyll plume. The 673/678-nm algorithm [Fig. 4(c)] yielded fair agreement over the offshore portion of the flight line but appears less sensitive to large scale chlorophyll variations within the nearshore plume area. Finally, the positively correlated 695/701-nm algorithm shows fair chlorophyll representation over most of the flight line.

Supporting surface chlorophyll concentration measurements made from the R/V Cape Henlopen indicated a range of 7.6 μg/liter in the region of the bay mouth to 0.08 μg/liter at the seaward end of the flight line. Clearly, the inner portion of the flight line would be considered to be Case II.[1] Outflow from tidal lagoons along the lower portion of the Delaware–Maryland–Virginia peninsula are injected into the coastal water during semidiurnal ebb tidal cycles through numerous inlets. Tidal plumes were visible from the aircraft at locations seaward of a number of these inlets. In normal late summer conditions the nutrient-rich water from the lagoons, which carries relatively high concentrations of phytoplankton, is confined to the inner portion of the shelf and transported south. In general, during late August, the discharge from the Chesapeake Bay flows south and typically does not extend far beyond the inner shelf.

Data from flight line *b* (see Fig. 1) was next processed for comparison with the results from flight line *a*. Flight line *b* can be considered nearshore, Case II coastal water, similar in a number of respects to the along-shore and inner shelf portions of flight line *a*. During the transit along the Delaware and New Jersey coastlines, the aircraft was flown in a zone from 2 to 5 km off the coast to conform with certain Department of Defense airspace flight restrictions. Numerous plumes extending from lagoonal inlets were crossed during this flight along the coast. Several well-developed fronts were also crossed at the entrance to Delaware Bay. Unlike flight line *a*, there were no offshore

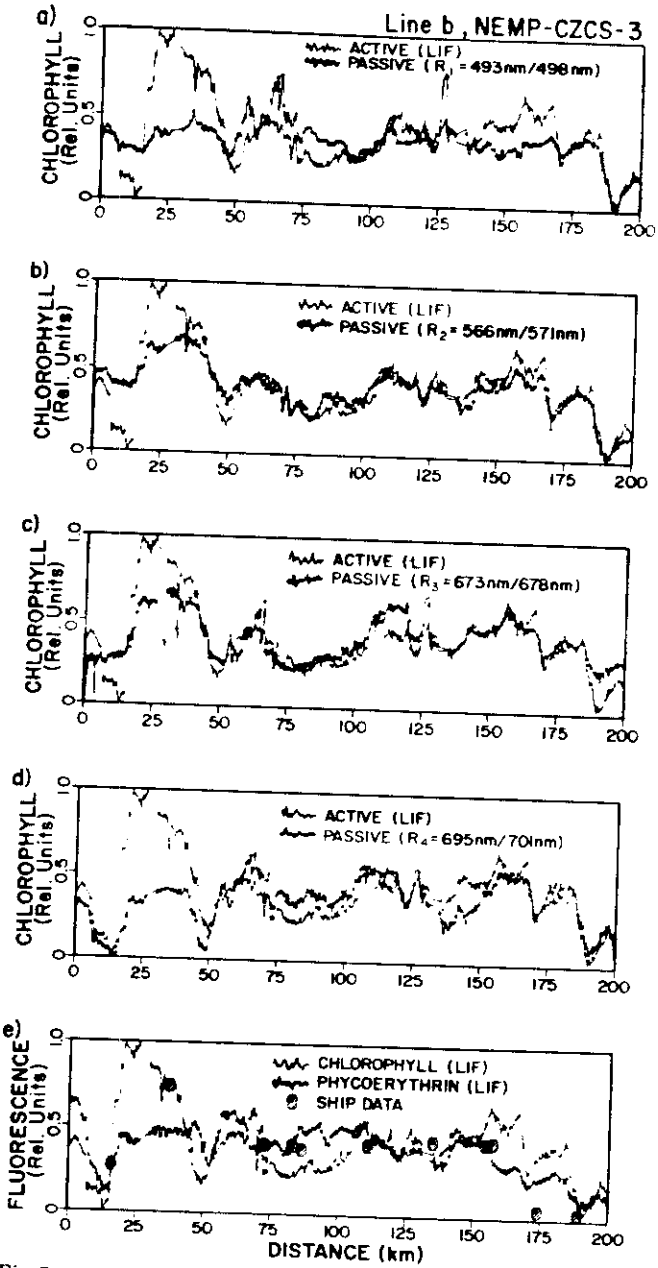

Fig. 5. (a)–(d) Along-track comparison of radiance ratios R_1, R_2, R_3, and R_4 with laser-induced chlorophyll fluorescence for flight line *b*. (e) Comparison of laser-induced phycoerythrin and chlorophyll fluorescence.

observations on flight line *b* which might be considered Case I.

Radiance-ratio results from flight line *b* are shown plotted in Figs. 5(a)–(d) using the same band combinations and format previously established for flight line *a*. Similarly, the log of the Raman normalized phycoerythrin and chlorophyll fluorescence values are plotted in Fig. 5(e). The large plume associated with the Delaware Bay outflow (between 15 and 45 km) is obvious within the figures as are the numerous large plumes associated with the outflows from lagoons along the New Jersey coastline. Log values of discrete surface truth chlorophyll values have been plotted in a visual best fit profile of unconnected larger symbols in Fig. 5(e). The surface truth chlorophyll values range from a low of 0.24 μg/liter near 190 km to a high of 13.4 μg/liter in the Delaware Bay outflow plume near 40 km. As was the case with flight line *a*, the surface truth sampling was not precisely coincident with the aircraft sampling line in either time or space. Spatial separations varied from ~4 to more than 10 km and temporal differences in time ranged from nearly 0 to more than 12 h. Accordingly, the surface truth chlorophyll values should again be primarily used to gauge the range of chlorophyll concentration, and the general distribution, rather than to determine the accuracy of individual lidar observations. The correlation coefficient for each of the radiance-ratio profiles in Figs. 5(a)–(d) are given in Table II along with the correlation coefficients for CZCS radiance-ratio band combinations. The computation of the correlation coefficients was constrained to the portion of the flight line between 50 and 200 km because of the relatively poor agreement found for all the band combinations when regressed with the chlorophyll fluorescence values over the entire flight line (including the region of the Delaware Bay outflow plume).

Reasonably good agreement with chlorophyll fluorescence was found for the 566/571- and 695/701-nm band combinations except in the vicinity of the Delaware Bay plume. Fair agreement was also obtained for the 493/498- and 695/701-nm band combinations, again except for the Delaware Bay plume. Band combinations that might resolve chlorophyll concentrations within the Bay plume and in the Bay proper could potentially be determined from a flight line oriented along the main axis of the bay.

Data acquired during the 1985 SEEP experiment (flight line *c* in Fig. 1) were next processed using the same methods. Ocean color spectra obtained on this flight line have previously yielded good correlation between laser-induced chlorophyll fluorescence and pigment estimates produced using a three-band spectral curvature algorithm.[36] The data collected on this pass are considered to be particularly valuable for use in ocean color algorithm testing with active–passive correlation spectroscopy because of the rather large range in chlorophyll concentration (<1 to ~8 μg/liter) and the presence of distinct areas of noncoherence between chlorophyll and phycoerythrin. The water type is more difficult for us to classify on the basis of the information which we have available. The flight line is located on the inner portion of the SEEP study site and a sustained west-to-east wind flow during the 24-h period preceding the experiment may have transported coastal water into the area. We, therefore, consider this experiment region to contain both Case I and II water types.

Relative chlorophyll values computed with the radiance-ratio algorithm using the same bands selected for flight lines *a* and *b* are shown plotted as cross sections in Figs. 6(a)–(d). The Raman corrected phycoerythrin fluorescence profile for flight line *c* is plotted in Fig. 6(e). The corresponding water Raman normal-

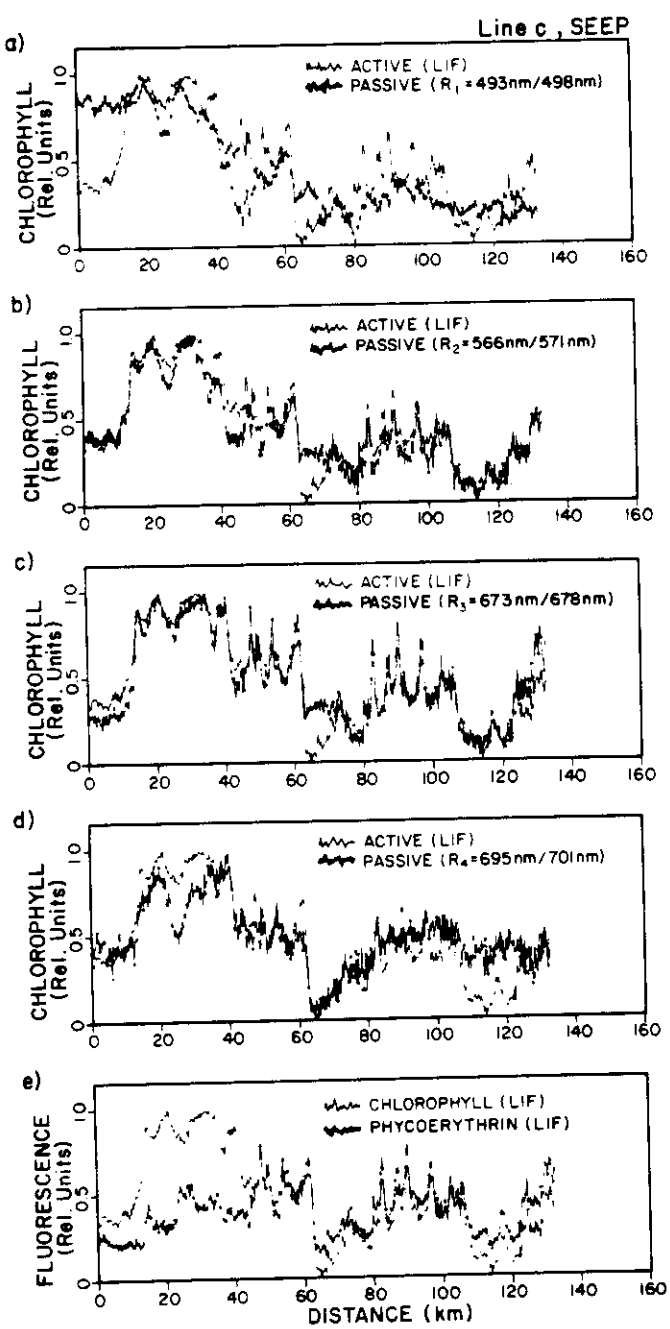

Fig. 6. (a)–(d) Along-track comparison of radiance ratios R_1, R_2, R_3, and R_4 with laser-induced chlorophyll fluorescence for flight line *c*. (e) Comparison of laser-induced phycoerythrin and chlorophyll fluorescence.

ized chlorophyll fluorescence profile is plotted in all the cross sections in Fig. 6. Again, the 566/571-nm radiance-ratio produced rather good agreement when compared to the laser-induced chlorophyll fluorescence. The 673/678-nm radiance-ratio algorithm shown in Fig. 6(c) also yielded good correlation with the laser-induced chlorophyll fluoresecence profile over most of the flight line. Lower agreement was found for the 493/498- and 695/701-nm band combinations. The 695/701-nm band combination also gave a noisier chlorophyll estimate probably due at least in

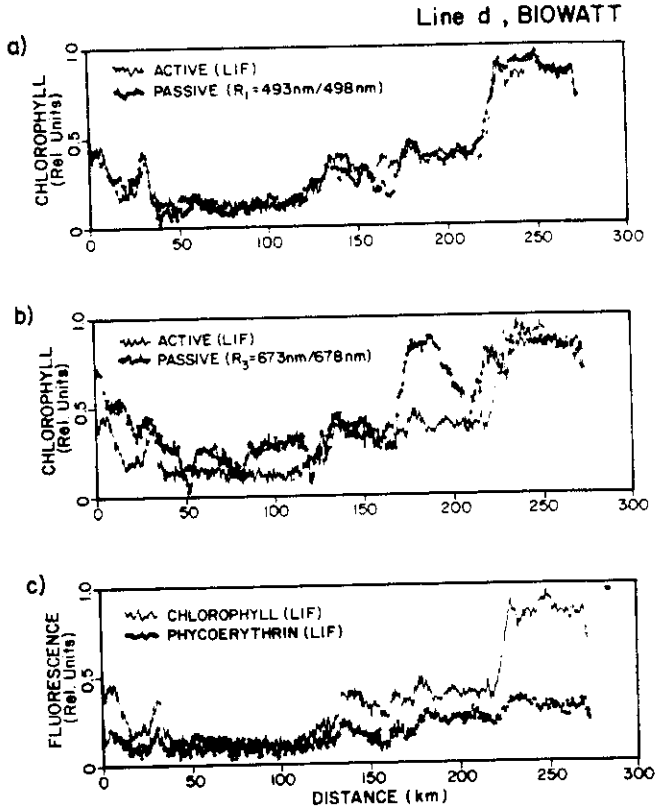

Fig. 7. (a)–(b) Along-track comparison of radiance ratios $R1$ and $R2$ with laser-induced chlorophyll fluorescence for flight line *d*. (c) Comparison of laser-induced phycoerythrin and chlorophyll fluorescence.

part to digitization granularity induced by the lower signal levels in the redder channels.

The correlation coefficients computed for each of the band combinations in Figs. 6(a)–(d) are provided in Table II. As shown in the table, the 566/571 algorithm [Fig. 6(b)] provided the best correlation with the Raman-normalized chlorophyll fluorescence data. The algorithm rather faithfully reproduces the laser-induced chlorophyll fluorescence except for a 10-km section beginning near 65 km. In this region and in other areas of minor disagreement, the passive algorithm overestimates the chlorophyll concentration relative to the laser fluorescence.

Flight line *d* on Fig. 1 from the BIOWATT field study was processed using the same techniques utilized in the analysis of the data sets from the NOAA CZCS/NEMP and SEEP experiments. Flight line *d* can be considered as representative of Case I waters. Figures 7(a) and (b) show cross sections comparing water Raman normalized chlorophyll fluorescence with relative pigment values computed using band combinations of 493/498 and 673/678 nm, respectively. The band combination located near 566/5471 nm did not produce usable results and was not plotted. During the BIOWATT experiment, the AOL fluorosensor spectrometer was adjusted to span a shorter-wavelength portion of the spectrum between 335 and 695 nm rather than the 409–769-nm wavelength setting

utilized for the NEMP/CZCS and SEEP missions. Accordingly, the positively correlated band combination located near 695/701 nm was not available in the BIOWATT data sets. The profile of the Raman corrected phycoerythrin fluorescence signal is compared with the chlorophyll fluorescence profile in Fig. 7(c). The best correlation between chlorophyll fluorescence and chlorophyll computed with the radiance-ratio algorithm was obtained using the 493/498-nm band combination shown in Fig. 7(a). This algorithm produced results which were in fairly good agreement in this blue water region where the chlorophyll concentration was judged from lidar signal strengths to have been $\geq 2\ \mu g$/liter. No ship truth was available for comparison to the airborne data. By contrast, the 673/678-nm band combination in Fig. 7(b) showed numerous departures from the laser-induced chlorophyll fluorescence over much of the flight line, especially in the 170–210-km region where the algorithm rather grossly overestimated the chlorophyll concentration.

VII. Summary and Conclusions

Two-band radiance-ratio algorithms in the visible spectrum have been evaluated for remote oceanic chlorophyll pigment determination using active–passive correlation spectroscopy techniques. Airborne active–passive (laser–solar) data from coastal, shelf-slope, and blue-water regions have been used to generate 2-D chlorophyll-fluorescence and radiance-ratio statistical correlation matrices containing all possible two-band combinations of the thirty-two available contiguous passive bands. The principal finding was that closely spaced radiance-ratio bands are highly correlated with laser-induced chlorophyll fluorescence within several distinct regions of the ocean color spectrum. Closely spaced radiance ratios were found to be particularly suitable for pigment recovery in near-coastal Case II waters. While, in most cases, wider spaced band combinations also produced good correlation with the chlorophyll fluorescence values (and even slightly higher correlation on flight line *c* obtained during the SEEP experiment), the benefits of utilizing closely space bands should be seriously considered in selecting bands for future ocean color sensors.

Closely spaced radiance-ratio algorithms possess certain advantages over widely spaced algorithms. First, for spaceborne applications the Rayleigh and aerosol atmospheric correction is very nearly the same for each of the closely spaced bands. For widely spaced bands the wavelength dependency of the atmospheric corrections can introduce additional errors in chlorophyll recovery, especially if the correction at one wavelength is extrapolated from another separated by a large-wavelength interval. Second, spaceborne sensors such as the Coastal Zone Color Scanner have discrete widely separated bands located in the blue and green spectral regions (e.g., 443, 520, 550 nm) which are used to determine pigment concentration. This instrument has exhibited a reduction in its radiometric sensitivity with time.[45,46] In particular, the blue band radiometric sensitivity decay has occurred at a steeper rate than the longer wavelength bands. For closely spaced bands the radiometric sensitivity decay would still have to be corrected, but in the case of closely spaced bands the decay could be approximately the same in each band. Thus errors due to differential radiometric sensitivity decay would be minimized. The separation of spectral bands in the AOL spectrometer is ~11.25 nm. Thus we cannot determine whether bands spaced more closely than 11.25 nm would further improve the results discussed in this paper. However, a practical limitation on minimum band separation arises from the fact that the radiance-ratio algorithm become noisier as the wavelength interval decreases.

The second significant finding from this study was that reasonably consistent performance was obtained from certain longer-wavelength band combinations, especially in Case II waters. These longer-wavelength band combinations also offer benefits that deserve consideration in the band selection process. For spaceborne sensors, operation at these longer wavelengths would provide a reduced atmospheric radiance contribution due to lower Rayleigh scatter. Unfortunately, this advantage would be partially offset by smaller water-leaving radiance in the orange-red spectral region. Additional modeling and high-altitude airborne experimental data are recommended to more fully understand and quantify the apparent advantages of closely spaced bands and especially their use in the orange-red spectral region. Some recent radiative transfer calculations seem to support some of the long-wavelength algorithm findings discussed herein. Using factor analysis, Fischer *et al.*[47] found that the natural fluorescence of phytoplankton chlorophyll *a* is detectable even in turbid coastal waters. Their modeling calculations showed that for coastal waters free of yellow substance (but with 1 km of boundary layer atmospheric turbidity) the chlorophyll fluorescence characteristic is still measurable.

Improved quantitative pigment measurements over the global oceans are limited by (a) lack of complete understanding of ocean color spectral variability, (b) the accuracy of atmospheric corrections, and (c) satellite sensor differential spectral degradation. In a modest way the work herein was meant to address all these concerns. Specifically, it is well known that virtually the entire ocean color spectrum is influenced or driven to some extent by the presence of chlorophyll-bearing phytoplankton. At any given oceanic location the spectral influence can be readily observed in radiance ratios of both widely spaced and closely spaced sensor bands. However, in spite of the very significient ocean color spectral variability in shelf and slope waters, we have found some degree of constancy within certain radiance-ratio spectral regions such as ~570, ~680, and ~700 nm.

Like some of our other algorithm investigations,[36] the results herein further suggest that significant information content resides within the ocean color spectrum. The major challenge is to interpret properly the findings revealed by the various algorithms and then to

improve further the accuracy of known analytical schemes.

The authors wish to extend their personal thanks to the many persons involved with the SEEP, NEMP-CZCS, and BIOWATT field experiment, the AOL project team, and aircraft operations personnel. We are particularly indebted to the Instrument Electro-Optics Branch for the loan of the frequency-doubled Nd:YAG laser used to obtain the active data. We also thank Curtiss Davis and the Ocean Processes Branch of NASA Headquarters for their continued support and encouragement. AOL system calibration assistance by the Sensor Evaluation Branch of GSFC and by Warren Hovis and Jack Knoll of the NOAA National Environment Satellite Data and Information Service as well as the field support of Catherine Warsh of the NOAA Ocean Assessments Division is gratefully acknowledged.

References

1. H. R. Gordon and A. Y. Morel, "Remote Assessment of Ocean Color for Interepretation of Satellite Visible Imagery," in *Lecture Notes on Coastal and Estuarine* (Springer-Verlag, New York, 1983).
2. R. R. Ramsey, "Study of the Remote Measurement of Ocean Color," Final Report, contract NASW-1658, TRW Corp, prepared for NASA, Washington, DC, 26 Jan. 1968.
3. N. G. Jerlov, "Significant Relationships Between Optical Properties of the Sea," in *Optical Aspects of Oceanography*, N. G. Jerlov and E. S. Nielsen, Eds. (Academic, New York, 1974), Chap. 4, pp. 77–94.
4. G. L. Clarke, G. C. Ewing, and C. J. Lorenzen, "Spectra of Backscattered Light from the Sea Obtained from Aircraft as a Measure of Chlorophyll Concentration," Science **167**, 1119 (1970).
5. G. L. Clarke and G. C. Ewing, "Remote Spectroscopy of the Sea for Biological Production Studies," in *Optical Aspects of Oceanography*, N. G. Jerlov and E. S. Nielsen, Eds. (Academic, New York, 1974), Chap. 17, pp. 389–413.
6. R. J. Curran, "Ocean Color Determination Through a Scattering Atmosphere," Appl. Opt. **11**, 1857 (1972).
7. J. C. Arvesen, J. P. Millard, and E. C. Weaver, "Remote Sensing of Chlorophyll and Temperature in Marine and Fresh Waters," in *Proceedings, Twenty-second International Astronautical Congress*, Brussels, Belgium (Publisher, Location, 1971).
8. J. C. Arvesen, J. P. Millard, and E. C. Weaver, "Remote Sensing of Chlorophyll and Temperature in Marine and Fresh Waters," Astronaut. Acta **18**, 229 (1974).
9. R. C. Ramsey and P. G. White, "Ocean Color Data Analysis Applied to MOCS and SIS Data," Final Report NOAA contract N62306-72-C-0037, 75 pp.
10. W. A. Hovis and K. C. Leung, "Remote Sensing of Ocean Color," Opt. Eng. **16**, 158 (1977).
11. J. D. H. Strickland, "The Estimation of Suspended Matter in Sea Water from the Air," unpublished paper (1962).
12. A. Morel and L. Prieur, "Analysis of Variations in Ocean Color," Limnol. Oceanogr. **22**, 709 (1977).
13. A. Morel and H. R. Gordon, "Report of the Working Group on Water Color," Boundary-Layer Meteorol. **18**, 343 (1980).
14. R. W. Austin, "The Remote Sensing of Spectral Radiance from Below the Ocean Surface," in *Optical Aspects of Oceanography*, N. G. Jerlov and E. S. Nielsen, Eds. (Academic, New York, 1974), Chap. 14, pp. 317–344.
15. H. R. Gordon, K. D. Clark, J. W. Brown, O. B. Brown, R. H. Evans, and W. W. Broenkow, "Phytoplankton Pigment Concentration in the Middle Atlantic Bight: Comparison of Ship Determinations and CZCS Estimates," Appl. Opt. **22**, 20 (1983).
16. F. E. Hoge and R. N. Swift, "Application of the NASA Airborne Oceanographer Lidar to the Mapping of Chlorophyll and Other Organic Pigments," in Chesapeake Bay Plume Study Superflux 1980, NASA Conf. Publ. 2188 (U.S. GPO, Washington, DC, 1981), pp. 349–374.
17. F. E. Hoge, and R. N. Swift, "Airborne Simultaneous Spectroscopic Detection of Laser-Induced Water Raman Backscatter and Fluorescence from Chlorophyll *a* and Other Naturally Occurring Pigments," Appl. Opt. **20**, 3197 (1981).
18. F. E. Hoge and R. N. Swift, "Airborne Dual Laser Excitation and Mapping of Phytoplankton Photopigments in a Gulf Stream Warm Core Ring," Appl. Opt. **22**, 2272 (1983).
19. F. E. Hoge and R. N. Swift, "Airborne Mapping of Laser-Induced Fluorescence of Chlorophyll *a* and Phycoerythrin in a Gulf Stream Warm Core Ring," in *Mapping Strategies in Chemical Oceanography*, A. Zirino, Ed., Advanced in Chemistry Series 209 (American Chemical Society, Washington, DC, 1985), Paper 18, pp. 353–372.
20. F. E. Hoge, R. E. Berry, and R. N. Swift, "Active–Passive Airborne Ocean Color Measurement: 1. Instrumentation," Appl. Opt. **25**, 39 (1986).
21. F. E. Hoge, R. N. Swift, and J. K. Yungel, "Active–Passive Airborne Ocean Color Measurement: 2. Applications," Appl. Opt. **25**, 48 (1986).
22. M. Bristow, D. Nielsen, D. Bundy, and F. Furtek, "Use of Water Raman Emission to Correct Airborne Laser Fluorosensor Data for Effects of Water Optical Attenuation," Appl. Opt. **20**, 2889 (1981).
23. R. C. Smith, U. California Santa Barbara; personal communication.
24. D. A. Kiefer, "Chlorophyll *a* Fluorescence in Marine Centric Diatoms: Responses of Chloroplasts to Light and Nutrient Stress," Mar. Biol. **23**, 39 (1973).
25. M. P. F. Bristow, D. H. Bundy, C. M. Edmonds, P. E. Pinto, B. E. Frey, and L. F. Small, "Airborne Laser Fluorosensor Survey of the Columbia and Snake Rivers: Simultaneous Measurements of Chlorophyll, Dissolved Organics and Optical Attenuation," Int. J. Remote Sensing **6**, 1707 (1985).
26. F. E. Hoge and R. N. Swift, "Experimental Feasibility of the Airborne Measurement of Absolute Oil Fluorescence Spectral Conversion Efficiency," Appl. Opt. **22**, 37 (1983).
27. F. E. Hoge and R. N. Swift, "Oil Film Thickness Measurement Using Airborne Laser-Induced Water Raman Backscatter," Appl. Opt. **19**, 3269 (1980).
28. F. E. Hoge and R. N. Swift, "Absolute Tracer Dye Concentration Using Airborne Laser-Induced Water Raman Backscatter," Appl. Opt. **20**, 1191 (1981).
29. F. E. Hoge and R. N. Swift, "Airborne Detection of Oceanic Turbidity Cell Structure Using Depth-Resolved Laser-Induced Water Raman Backscatter," Appl. Opt. **22**, 3378 (1983).
30. F. E. Hoge, R. N. Swift, and E. B. Frederick, "Water Depth Measurement Using an Airborne Pulsed Neon Laser System," Appl. Opt. **19**, 871 (1980).
31. F. E. Hoge, W. B. Krabill, and R. N. Swift, "The Reflection of UV Laser Pulses from the Ocean," Mar. Geod. **8**, 313 (1984).
32. J. L. Bufton, F. E. Hoge, and R. N. Swift, "Airborne Measurements of Laser Backscatter from the Ocean Surface," Appl. Opt. **22**, 2603 (1983).
33. W. B. Krabill, J. G. Collins, L. E. Link, R. N. Swift, and M. L. Butler, "Airborne Laser Topographic Mapping Results," Photogramm. Eng. Remote Sensing **50**, 685 (1984).

34. R. Nelson, W. B. Krabill, and G. Maclean, "Determining Forest Canopy Characteristics Using Airborne Laser Data," Remote Sensing Environ. 15, 201 (1984).
35. F. E. Hoge, R. N. Swift, and J. K. Yungel, "Feasibility of Airborne Detection of Laser-Induced Fluorescence Emissions from Green Terrestrial Plants," Appl. Opt. 22, 2991 (1983).
36. F. E. Hoge and R. N. Swift, "Active–Passive Correlation Spectroscopy: A New Technique for Identifying Ocean Color Algorithm Spectral Regions," Appl. Opt. 25, 2571 (1986).
37. J. Marra and E. Hartwig, "BIOWATT: A Study of Bioluminescence and Optical Variability in the Sea," Eos 65, 732 (1984).
38. G. W. Grew and L. S. Mayo, "Ocean Color Algorithm for Remote Sensing of Chlorophyll," NASA Tech. Paper 2164 (Langley Research Center, Hampton, VA, 1983).
39. G. W. Grew, "Real-Time Test of MOCS Algorithm During Superflux 1980," in Chesapeake Bay Plume Study Superflux 1980, NASA Publ. 2188 (U.S. GPO, Washington, DC, 1981).
40. J. W. Campbell and W. E. Esaias, "Basis for Spectral Curvature Algorithms in Remote Sensing of Chlorophyll," Appl. Opt. 22, 1084 (1983).
41. A. Morel, "In-Water and Remote Measurements of Ocean Color," Boundary-Layer Meteorol. 18, 177 (1980).
42. S. Q. Duntley, R. W. Austin, W. H. Wilson, C. F. Edgerton, and M. E. Moran, "Ocean Color Analysis," Visibility Laboratory of the Scripps Institution of Oceanography Report S10 Ref. 74-10 (1974).
43. M. B. Bristow, D. Nielsen, D. Bundy, and R. Furtek, "Use of Water Raman Emission to Correct Airborne Laser Fluorosensor Data for Effects of Water Optical Attenuation," Appl. Opt. 20, 2889 (1981).
44. J. W. Campbell, "An Algorithm for Computing Chlorophyll *a* Concentrations Using Dual Frequency Flourosensor," in Chesapeake Bay Plume Study, Superflux 1980, NASA Conf. Publ. 2188 (U.S. GPO, Washington, DC, 1981), p. 417.
45. H. R. Gordon, J. W. Brown, D. B. Brown, R. H. Evans, and D. K. Clarke, "NIMBUS 7 CZCS: Reduction of Its Radiometric Sensitivity with Time," Appl. Opt. 22, 3929 (1983).
46. J. L. Mueller, "NIMBUS 7 CZCS: Confirmation of Its Radiometric Sensitivity Decay Rate Through 1982," Appl. Opt. 24, 1043 (1985).
47. J. Fischer, R. Doerffer, and H. Grassl, "Factor Analysis of Multispectral Radiances Over Coastal and Open Ocean Water Based on Radiative Transfer Calculations," Appl. Opt. 25, 448 (1986).